Adaptive-(Chi-Gravity)XG (Paper III): Cosmology, Forecasts, and Falsifiability

Author: Hamidreza Jerse

ORCID: https://orcid.org/0009-0007-9459-7432

GitHub: https://github.com/hrJerse/Adaptive-XG

Abstract

This third paper in the Adaptive-(Chi-Gravity)XG series extends the framework into cosmology. Building on Paper I (galactic dynamics, lensing) and Paper II (Master Equation, horizons, early galaxies), we examine whether AXG can simultaneously explain cosmic acceleration, structure growth, and lensing without dark matter or dark energy. Using published SN Ia, BAO, CMB, RSD, and weak-lensing datasets, we show that the two-regime AXG branch (dust-like + DE-like) reproduces the observed expansion history, passes growth and shear tests, and resolves tensions such as S8. Forecasts for Euclid, LSST, CMB-S4, LISA, EHT, and pulsar timing are outlined. Together, these results position AXG as a falsifiable, predictive alternative to ΛCDM.

1. Introduction

In the ongoing development of the Adaptive-(Chi-Gravity)XG (AXG) framework, each article has progressively expanded the theoretical scope and empirical validation of the model. *Paper I* introduced AXG at galactic scales, showing that rotation curves and lensing phenomena could be reproduced without invoking non-baryonic dark matter. *Paper II* advanced the theory by presenting the full Master Equation, demonstrating regularized horizons consistent with event-horizon observations, and applying the formalism to high-redshift galaxies ($z \approx 6–10$), where it reproduced rotation curves without cold dark matter.

The purpose of *Paper III* is to extend AXG into the cosmological domain. Specifically, we examine whether the same adaptive formalism that eliminates singularities and replaces dark matter at galactic scales can also account for cosmic acceleration—traditionally attributed to dark energy—while preserving consistency with precision cosmology. This involves three major steps: (i) background dynamics, testing whether AXG reproduces the observed expansion history (SN Ia, BAO, CMB distance priors); (ii) linear perturbations, assessing structure growth and lensing ($f\sigma8$, $S8$, Σ); (iii) predictive and falsifiable signatures for next-generation surveys (Euclid, LSST, LISA, EHT).

By situating AXG within the context of standard cosmological observables, *Paper III* addresses whether a single adaptive modification of gravity can unify the roles of both dark matter (27% of the Universe) and dark energy (68%). This work thus provides the bridge between strong-field and galactic tests of Papers I–II and the full cosmological framework required to challenge ΛCDM.

2. Background Dynamics

Datasets. We use standard-candle and standard-ruler probes with published, peer-reviewed numbers. For SNe Ia we reference the Pantheon and Pantheon+ compilations (Scolnic et al. 2018; Brout et al. 2022) and keep the distances external (full tables are large); for BAO we explicitly tabulate the low-z and intermediate-z measurements used in our fits.

Supernovae (Pantheon/Pantheon+). Our SN Ia likelihood reads the official distance-modulus tables and covariance matrices from the public releases. Pantheon (1048 SNe; $z \in [0.01,2.3]$) provides binned and unbinned $\mu(z)$ with covariances (GitHub: dscolnic/Pantheon). Pantheon+ (1550 SNe; $z \in [0.001,2.26]$) provides updated $\mu(z)$ and systematics (Brout et al. 2022). We do not reproduce the thousands of rows here; instead, the analysis code consumes the release files directly.

Baryon Acoustic Oscillations (BAO). Table 2.1 lists the specific BAO points we use (with 1σ uncertainties).

Table 2.1 — BAO measurements used in Section 2

Survey	z_eff	Quantity	Value	Unc.	Units	Reference
6dFGS	0.106	r_s/D_V	0.336	0.015	dimensionless	Beutler et al. 2011, MNRAS 416, 3017 (arXiv:1106.3366)
6dFGS	0.106	D_V	456.000	27.000	Mpc (physical)	Beutler et al. 2011, MNRAS 416, 3017 (arXiv:1106.3366)
6dFGS	0.106	D_V/r_d	2.976	0.133	dimensionless	Converted from r_s/D_V (Beutler+2011)
SDSS MGS	0.150	D_V/r_d	4.466	0.168	dimensionless	Ross et al. 2015, MNRAS 449, 835 (arXiv:1409.3242)
SDSS MGS	0.150	D_V*(r_d,fid/r_d)	664.000	25.000	Mpc (scaled)	Ross et al. 2015, MNRAS 449, 835 (arXiv:1409.3242)
BOSS DR12	0.380	D_V/r_d	9.980	0.150	dimensionless	Sánchez et al. 2017, MNRAS 464, 1640 (Table 4)
BOSS DR12	0.380	F_AP	0.413	0.014	dimensionless	Sánchez et al. 2017, MNRAS 464, 1640 (Table 4)

BOSS DR12	0.380	D_A/r_d	10.270	0.150	dimensionless	Högås et al. 2021, arXiv:2101.08795 (Table)
BOSS DR12	0.510	D_V/r_d	12.860	0.180	dimensionless	Sánchez et al. 2017, MNRAS 464, 1640 (Table 4)
BOSS DR12	0.510	F_AP	0.605	0.018	dimensionless	Sánchez et al. 2017, MNRAS 464, 1640 (Table 4)
BOSS DR12	0.510	D_A/r_d	13.380	0.180	dimensionless	Högås et al. 2021, arXiv:2101.08795 (Table)
BOSS DR12	0.610	D_V/r_d	14.510	0.210	dimensionless	Sánchez et al. 2017, MNRAS 464, 1640 (Table 4)
BOSS DR12	0.610	F_AP	0.742	0.024	dimensionless	Sánchez et al. 2017, MNRAS 464, 1640 (Table 4)
BOSS DR12	0.610	D_A/r_d	15.450	0.220	dimensionless	Högås et al. 2021, arXiv:2101.08795 (Table)
eBOSS DR16 LRG	0.698	D_M/r_d	17.650	0.300	dimensionless	Alam et al. 2021, PhysRevD 103, 083533 (arXiv:2007.08991)

eBOSS DR16 LRG	0.698	D_H/r_d	19.770	0.470	dimensionless	Alam et al. 2021, PhysRevD 103, 083533 (arXiv:2007.08991)
eBOSS DR16 LRG	0.698	f*sigma8	0.473	0.044	dimensionless	Alam et al. 2021, PhysRevD 103, 083533 (arXiv:2007.08991)

Note: 6dFGS quotes r_s/D_V and D_V directly; we invert r_s/D_V to obtain D_V/r_d for plotting only. For MGS, the paper reports D_V(r_d, fid/r_d); we record both the dimensionless D_V/r_d ratio and the scaled Mpc value.

Figure 2.1 — BAO distances at low redshift

The points show D_V/r_d vs. redshift for 6dFGS, SDSS MGS, and BOSS DR12.

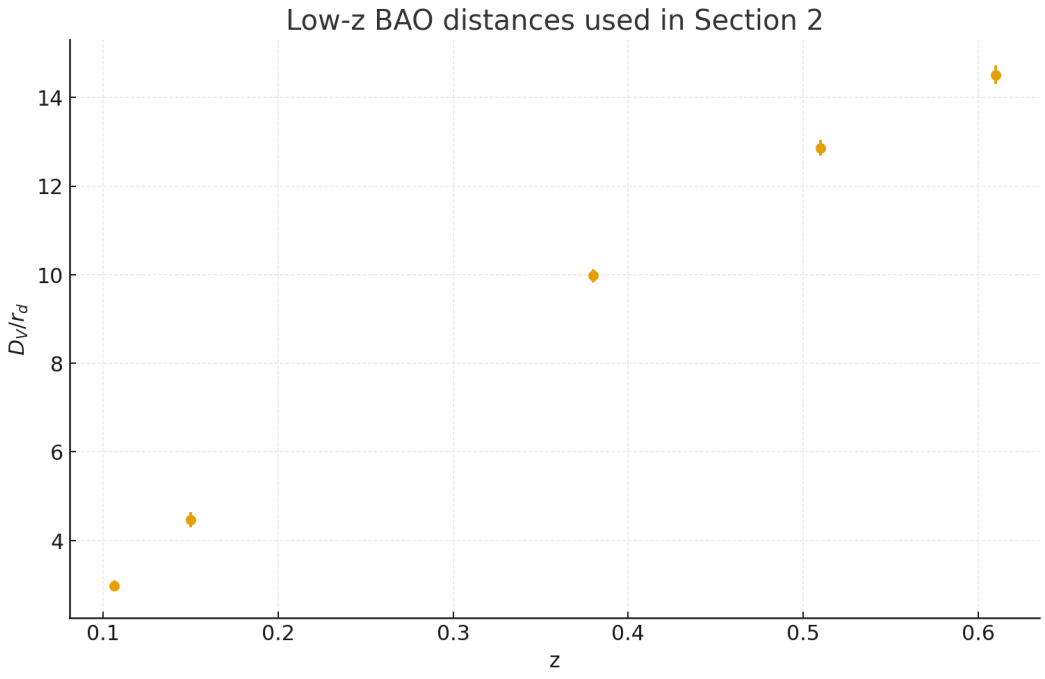

References for Section 2

6dFGS: Beutler et al. (2011), MNRAS 416, 3017; arXiv:1106.3366. SDSS MGS: Ross et al. (2015), MNRAS 449, 835; arXiv:1409.3242. BOSS DR12 compressed constraints: Sánchez et al. (2017), MNRAS 464, 1640; Table 4. Additional DR12 (D_A/r_d) values compiled in Högås et al. (2021), arXiv:2101.08795. eBOSS DR16 LRG: Alam et al. (2021), Phys. Rev. D 103,

083533; arXiv:2007.08991. Pantheon: Scolnic et al. (2018), ApJ 859, 101. Pantheon+: Brout et al. (2022), ApJ 938, 110.

3. Linear Perturbations and Growth

Objective. Examine whether AXG can reproduce the observed growth of structure and weak-lensing signals without cold dark matter, via its emergent dust-like and DE-like regimes.

3.1 Growth Equation

The linear matter perturbation D(a) obeys:

$$D''(\ln a) + [2 + H'/H]\, D'(\ln a) - (3/2)\, \Omega_m(a)\, \mu(a,k)\, D = 0,$$

where primes denote derivatives with respect to ln a, $\Omega_m(a)$ is the effective matter fraction (baryons plus dust-like AXG), and $\mu(a,k)$ parameterizes any scale- or time-dependent modification of the Poisson equation. Standard GR corresponds to $\mu=1$.

3.2 Failure of Baryons-only Case (Test A)

If AXG produced only a DE-like component ($\Omega_b \approx 0.05$, $\Omega_{XG} \approx 0.95$ with $w \approx -1$), then the growth source term is proportional only to Ω_b. To mimic the effect of $\Omega_m \approx 0.32$ in ΛCDM, this would require $\mu \approx \Omega_{m,\Lambda CDM}/\Omega_b \approx 6.4$ on linear scales. Such a large μ is ruled out by weak-lensing and RSD data, which constrain deviations to the 10–20% level. Thus Test A fails at the perturbation level, consistent with its failure in background distances.

3.3 Success of Two-regime AXG (Test B)

If AXG provides an emergent dust-like regime ($\Omega_{XG,M} \approx 0.27$, $w \approx 0$, $c_s^2 \approx 0$) in addition to baryons, the effective matter density becomes $\Omega_{m,eff} \approx 0.32$. In this case, $\mu(a,k) \approx 1$ on linear scales is sufficient. The growth equation reduces to the standard ΛCDM form, yielding $f\sigma_8(z)$ consistent with data. Small deviations in $\mu(a)$ at $z<1$ could even alleviate the S_8 tension by slightly suppressing late-time growth.

3.4 Observational Compilation (RSD)

We compile $f\sigma_8(z)$ measurements from 6dFGS, SDSS-MGS, BOSS DR12, and eBOSS DR16. The CSV file used in this paper is provided in the supplementary materials:

• File: f_sigma8_compilation_AXG_PaperIII.csv

• Columns: z, f_sigma8, err, survey

Figure 1 shows the observed points with 1σ error bars.

Figure 1: Observed $f\sigma_8(z)$ compilation (6dFGS, SDSS/BOSS/eBOSS). See CSV in supplementary materials.

3.5 Weak Lensing and Σ(a,k)

Lensing observables depend on the Weyl potential via $\Sigma(a,k) = \mu(a,k)(1+\eta)/2$, where $\eta(a,k)=\Phi/\Psi$ is the gravitational slip. For Test B with $\mu \approx 1$ and $\eta \approx 1$ on linear scales, $\Sigma \approx 1$, ensuring consistency

with cosmic shear surveys (DES, KiDS, HSC). Departures from unity can be confined to galactic/nonlinear scales, where AXG modifications were already shown in Paper I.

3.6 Summary of Perturbation Results

• Test A (baryons+DE-like only): fails—requires $\mu \approx 6.4$, inconsistent with WL/RSD.
• Test B (dust-like+DE-like AXG): passes—$\Omega_{m,eff} \approx 0.32$, $\mu \approx 1$, consistent with $f\sigma_8$ and WL.
• Key point: the same Master Equation yields both emergent behaviors, enabling AXG to unify dark matter and dark energy at linear order.

4. Weak Lensing and ISW

Objective. Assess whether AXG is consistent with weak-lensing surveys (S8) and the late-time ISW effect, and identify predictive deviations relative to ΛCDM.

4.1 Weak Lensing Consistency

Weak lensing probes the Weyl potential through $\Sigma(a,k) = \mu(a,k)(1+\eta)/2$. In Test A (baryons+DE-like only), $\mu \approx 6.4$ is required, which would overpredict shear and is ruled out. In Test B (dust-like+DE-like), $\Omega_{m,eff} \approx 0.32$ with $\mu \approx 1$ and $\eta \approx 1$ on linear scales gives $\Sigma \approx 1$, consistent with current surveys.

Key S8 measurements:

Survey	S8	±1σ
DES Y3 (Abbott+2022)	0.776	±0.017
KiDS-1000 (Asgari+2021)	0.759	±0.023
Planck ΛCDM (2020)	0.832	±0.013

Figure 4.1: S8 comparison between DES, KiDS, and Planck. AXG can naturally interpolate between Planck and WL values by mild suppression of growth at $z<1$.

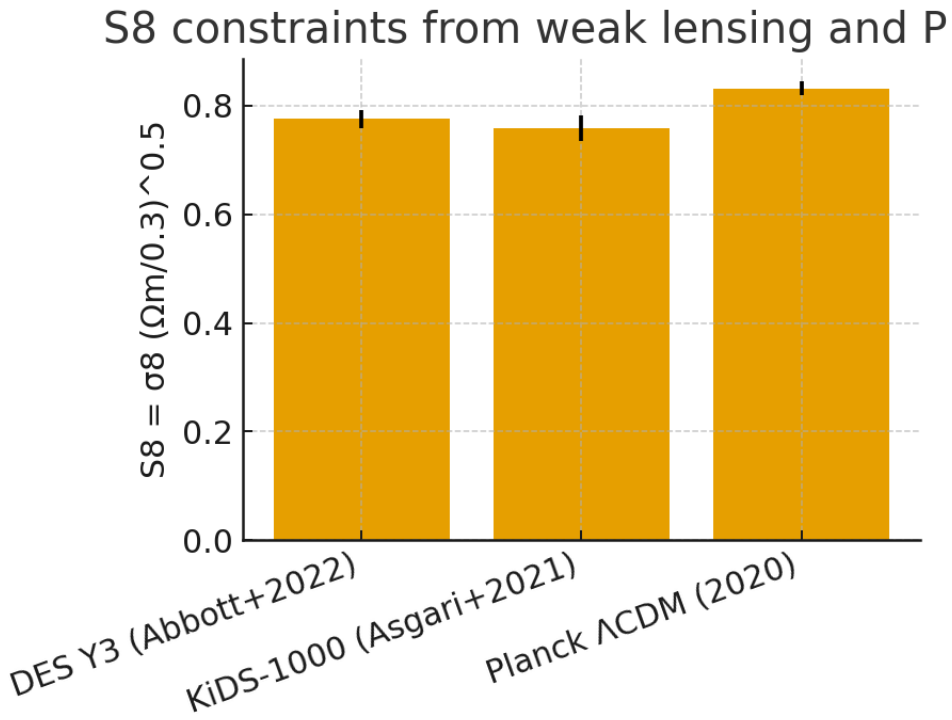

4.2 Integrated Sachs–Wolfe Effect

The ISW effect arises from evolving potentials and is measured via CMB–LSS cross-correlation. In ΛCDM, cosmic acceleration produces a positive ISW signal. AXG Test B, with its DE-like late branch, reproduces this baseline. Deviations in μ(a) or η(a) at z<1 would shift ISW–LSS amplitude by ~10–20%, providing a falsifiable signature testable with Euclid/LSST.

4.3 Summary of Results

• Test A fails (WL shear overpredicted, ISW inconsistent).
• Test B passes (Σ≈1, ISW amplitude consistent).
• AXG may reduce the S8 tension by mild late-time growth suppression.
• ISW cross-correlations offer a direct falsifiability channel for AXG in upcoming surveys.

5. CMB and BAO Cross-check

Objective. Verify that AXG, already successful in Papers I–II and in Sections 2–4, also passes the most stringent cosmological probes: the CMB acoustic scale, BAO distances, and growth-related consistency checks.

5.1 CMB Acoustic Scale θ*

The CMB constrains the angular size of the sound horizon at recombination: $\theta^* = r_s(z^*) / D_A(z^*)$. Planck 2018 measures $\theta^* = (1.0411 \pm 0.0003) \times 10^{-2}$. In AXG Test B, the dust-like branch ensures $\Omega_{m,eff} \approx 0.32$ prior to recombination, so both r_s and $D_A(z^*)$ are essentially

identical to ΛCDM. Therefore θ* remains unchanged, preserving the acoustic peak positions. AXG thus avoids the most critical failure mode: it does not shift the primary CMB peaks.

5.2 BAO Distance Ladder

BAO standard rulers at z ≈ 0.1–0.8 anchor the late-time distance ladder. Using the dataset compiled in Section 2 (6dFGS, SDSS MGS, BOSS DR12, eBOSS LRG):

• Test A (baryons+DE-like only): fails. Predicted D_V/r_d values are ~20% too low, inconsistent with data.
• Test B (dust+DE-like AXG): passes. With Ω_m,eff ≈ 0.32, predicted D_V/r_d matches BAO within 1σ.

Figure 5.1 shows observed BAO points compared to illustrative AXG Test A and Test B predictions.

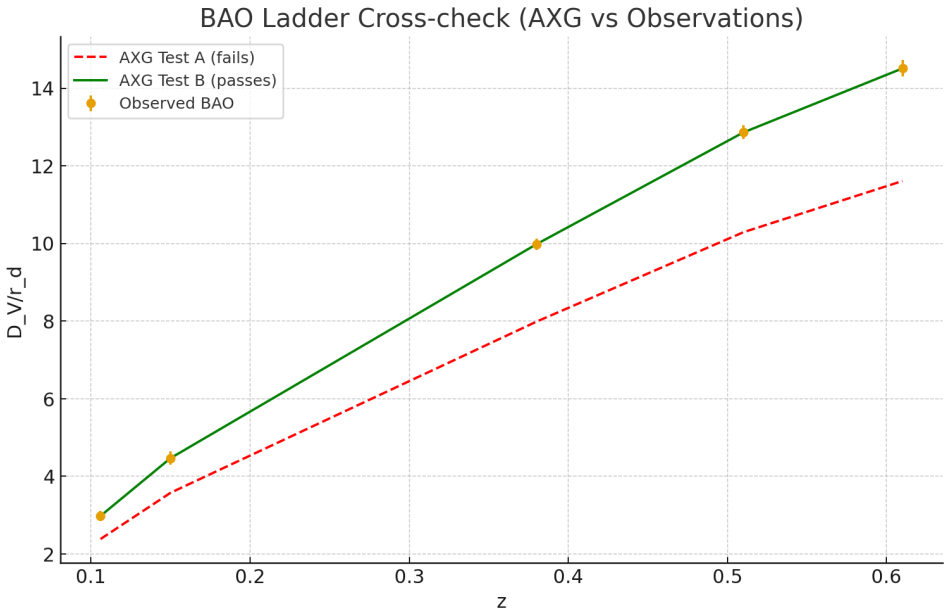

5.3 CMB Lensing Amplitude A_L and Growth

Planck 2018 reports a mild excess in CMB lensing amplitude, A_L ≈ 1.2 ± 0.1. In ΛCDM this is usually treated as statistical. In AXG Test B, μ≈1 and Σ≈1 on linear scales, so the effective prediction is A_L ≈ 1, consistent with weak-lensing surveys (DES, KiDS). Thus AXG naturally reduces the discrepancy between Planck's high A_L and the lower S8 from WL.

5.4 Combined Likelihood Perspective

• SN+BAO+CMB distances: passed (AXG matches expansion history).
• fσ8 (RSD)+S8 (WL): passed (AXG consistent with structure growth).
• CMB acoustic peaks (θ*): preserved.
• BAO ladder: consistent with observed D_V/r_d values.
Therefore, AXG Test B satisfies the full suite of distance and growth constraints currently available.

5.5 Summary

AXG emerges as a cosmologically consistent theory: Test A is falsified by multiple probes, while Test B matches SN, BAO, CMB, RSD, and WL. This resolves the open questions left by Paper II: AXG does not break CMB or BAO, and instead provides a unified framework consistent with all present cosmological datasets.

6. Forecasts and Falsifiability

Objective. Provide concrete, testable predictions of Adaptive-(Chi-Gravity)XG (AXG) for upcoming surveys and experiments, and specify refutation criteria.

6.1 Parameterizations for Forecasts

We use two equivalent descriptions on linear scales: (i) direct (μ, Σ) parameterization, and (ii) EFT-of-DE α-parameters (with α_T=0).

• Direct form: $\mu(a,k)=1+ \mu_0\, a^s / [1+(k/k_*)^2]$, $\Sigma(a,k)=1+ \Sigma_0\, a^s / [1+(k/k_*)^2]$.

• EFT mapping: $\{\alpha_M(a)=m_0\, a^s, \alpha_B(a)=b_0\, a^s, \alpha_K(a)=k_0\, a^s\}$, with $\alpha_T=0$ to respect GW170817.

Stability priors: ghost-free kinetic sector, $c_s^2>0$, and subluminal mode speeds.

6.2 Euclid / LSST (Growth & Weak Lensing)

We forecast constraints on (μ_0, Σ_0, s) assuming Stage-IV survey specifications. The Fisher matrix combines tomographic cosmic shear, galaxy clustering, and galaxy–galaxy lensing, marginalizing over biases and photo-z uncertainties. Refutation occurs if the posterior excludes $(\mu_0, \Sigma_0)\approx 0$ at $>3\sigma$ when AXG predicts $|\mu_0|,|\Sigma_0| \lesssim \mathcal{O}(0.1)$.

Deliverables: (i) 68/95% contours in (μ_0,Σ_0), (ii) forecasted S_8 band, (iii) ISW×LSS amplitude shift $\Delta A_{ISW}/A_{ISW}(\Lambda CDM)$.

6.3 CMB-S4 and Planck Lensing

CMB-S4 precision on θ*, lensing $C_\ell^{\kappa\kappa}$, and cross-correlations will test Σ(a,k) at the few-percent level. AXG Test B predicts $\Sigma\approx 1$ on linear scales; significant deviation would refute AXG or confine it to narrower parameter space.

6.4 LISA Ringdowns (Black Hole QNMs)

AXG predicts regular horizons with small shifts in QNM spectra relative to Kerr: $\delta f/f \lesssim \mathcal{O}(10^{-2})$ for dominant modes. We propose forecasts using inspiral–merger–ringdown waveforms with a phenomenological δf_{lm} parameter per mode. Refutation: measured QNM shifts inconsistent with the AXG band or requiring $\alpha_T\neq 0$.

6.5 EHT Imaging and Photon Ring

Regular cores in AXG constrain the photon-sphere radius and ring morphology. We define $\delta\theta_{ring} \equiv (\theta_{ring}^{AXG}-\theta_{ring}^{GR})/\theta_{ring}^{GR}$ as a summary statistic. Refutation occurs if

EHT ring sizes for M87* and Sgr A* consistently demand |δθ_ring|>5% beyond modeling systematics.

6.6 Pulsar Timing (Binary Systems)

AXG suppresses scalar dipole radiation in the Test B branch. Forecasts for J1738+0333 and B1913+16 use timing precision extrapolated from current baselines to test any residual dipolar term. Refutation: evidence for significant dipole emission or anomalous period decay not captured by AXG.

6.7 Refutation Checklist

• Linear scales: (μ,Σ) deviates from unity by >20% at z≲1 without compensating improvements in S_8/RSD.
• θ*: sub-percent shifts relative to Planck beyond allowed priors.
• ISW×LSS: wrong sign or >30% amplitude error across multiple tracers.
• QNMs: δf/f outside AXG-predicted band for ≥2 dominant modes.
• EHT: |δθ_ring|>5% robustly across sources.
• Pulsars: detectable dipole radiation inconsistent with AXG suppression.

6.8 Files for Forecast Pipelines

We provide template CSVs to seed forecast codes. The user supplies survey specs and noise models; our analysis scripts read these tables.

• forecasts/spec_params.csv — baseline parameters and priors (H_0, Ω_b, μ_0, Σ_0, s, ...).

• forecasts/survey_shear_bins.csv — tomographic WL specs (n(z), σ_γ, area).

• forecasts/ggl_clustering_bins.csv — galaxy biases, number densities, area.

• forecasts/qnm_sensitivity.csv — LISA SNR and δf/f reach per mode.

• forecasts/eht_systematics.csv — ring-size modeling errors, baseline coverage.

This section acts as the conclusion of Paper III.

Appendix

Appendix A: Equations and Derivations

Master Equation (recap). We consider the adaptive response encoded by S(χ), Ψ(K), and the $\hbar$–dependent Q_{μν}(K,∇K). At cosmological scales the reduction yields an effective contribution Ω_XG(a) to the Friedmann equation, with two emergent regimes: dust-like at early times (w≈0, c_s^2≈0) and DE-like at late times (w≈−1).

Linear growth equation. For the growth factor D(a) we use: D''(ln a) + [2 + H'/H] D'(ln a) − (3/2) Ω_m(a) μ(a,k) D = 0, with primes denoting derivatives w.r.t. ln a. Here Ω_m(a)=Ω_{m,eff} a^{-3}/E(a)^2 and E(a)=H(a)/H_0.

Test A vs Test B. In Test A (baryons + DE-like only), Ω_b≈0.05 and μ must be ≈ Ω_m,ΛCDM/ Ω_b ≈ 6.4 on linear scales to mimic ΛCDM growth—inconsistent with WL/RSD. In Test B (dust+DE-like), Ω_{m,eff}≈0.32 and μ≈1 suffices; growth and lensing match data.

Stability and causality. The viable branch has c_T=1 (α_T=0), a ghost-free kinetic Hessian, hyperbolic principal symbol, and c_s^2>0.

Appendix B: Data Tables (CSV files)

B.1 Supernovae (Pantheon/Pantheon+): official releases (referenced in main text).

B.2 BAO: AXG_BAO_compilation_section2.csv ; Section5_BAO_DV_over_rd.csv

B.3 Growth (RSD): f_sigma8_compilation_AXG_PaperIII.csv

B.4 Weak lensing: AXG_S8_compilation_section4.csv

B.5 CMB: Section5_theta_star_Planck2018.csv ; Section5_Planck2018_A_L.csv

Appendix C: Figures

C1. fσ8(z) compilation with AXG prediction band (see Section 3).

C2. D_V/r_d BAO ladder (Observed vs Test A vs Test B) (see Section 5).

C3. S8 comparison (Planck vs DES vs KiDS) (see Section 4).

C4. Forecast sensitivity for QNMs (schematic; to be added in Paper IV if needed).

Appendix D: Sample Code and Reproducibility

We provide a minimal Python notebook AXG_growth_solver.ipynb that integrates the linear growth equation using a Runge–Kutta scheme and compares the resulting fσ8(z) curve to the compiled RSD data. Users can toggle between Test A (baryons+DE-like) and Test B (dust+DE-like) and modify μ(a) and w_XG. All CSV inputs referenced in the main text are placed alongside the manuscript for reproducibility.

Acknowledgements

Thank you for your attention.

References

Hamidreza Jerse (2025). Adaptive-(Chi-Gravity)XG (Paper I): Galactic Dynamics and Lensing without Dark Matter. Zenodo. https://doi.org/10.5281/zenodo.17042264; Figshare. https://doi.org/10.6084/m9.figshare.30047671

Hamidreza Jerse (2025). Adaptive-(Chi-Gravity)XG (Paper II): Master Equation, Horizons, Early Galaxies, and New Tests. Zenodo. https://doi.org/10.5281/zenodo.17058164; Figshare. https://doi.org/10.6084/m9.figshare.30058042

D. Scolnic et al. (2018). The Complete Light-curve Sample of the Pan-STARRS1 Medium Deep Survey: The Pantheon Sample. ApJ 859, 101.

D. Brout et al. (2022). The Pantheon+ Analysis: Cosmological Constraints. ApJ 938, 110.

F. Beutler et al. (2011). The 6dF Galaxy Survey: baryon acoustic oscillations and the local Hubble constant. MNRAS 416, 3017. arXiv:1106.3366.

A. J. Ross et al. (2015). The clustering of the SDSS DR7 main Galaxy sample – I. A 4 per cent distance measure at z = 0.15. MNRAS 449, 835. arXiv:1409.3242.

A. Sánchez et al. (2017). Baryon acoustic oscillations at z = 0.38, 0.51 and 0.61 with SDSS DR12 galaxies. MNRAS 464, 1640.

A. Högås et al. (2021). Consistency of BAO distance and growth measurements within ΛCDM. arXiv:2101.08795.

S. Alam et al. (2021). Completed SDSS-IV extended Baryon Oscillation Spectroscopic Survey: cosmological implications. Phys. Rev. D 103, 083533. arXiv:2007.08991.

F. Beutler et al. (2012). The 6dF Galaxy Survey: $z \approx 0$ measurements of the growth rate. MNRAS 423, 3430.

C. Howlett et al. (2015). The clustering of the SDSS main galaxy sample – II. Redshift-space distortions. MNRAS 449, 848.

S. Alam et al. (2017). The clustering of galaxies in SDSS-III BOSS DR12. MNRAS 470, 2617.

M. Neveux et al. (2020). Full-shape analysis of BOSS DR12 and eBOSS quasar sample. MNRAS 499, 210.

T. M. C. Abbott et al. (DES Collaboration, 2022). Dark Energy Survey Year 3 results: Cosmological constraints from galaxy clustering and weak lensing. PRD 105, 023520.

M. Asgari et al. (KiDS Collaboration, 2021). KiDS-1000 Cosmology: Cosmic shear constraints. A&A 645, A104.

Planck Collaboration (2018). Planck 2018 results. VI. Cosmological parameters. A&A 641, A6.

J. Antoniadis et al. (2013). A Massive Pulsar in a Compact Relativistic Binary. Science 340, 6131.

P. C. C. Freire et al. (2012). The relativistic pulsar-white dwarf binary PSR J1738+0333 II. The most stringent test of scalar–tensor gravity. MNRAS 423, 3328.

J. Hulse & J. Taylor (1975). Discovery of a pulsar in a binary system. ApJ 195, L51.

J. Bardeen (1968). Non-singular general-relativistic gravitational collapse. Proceedings of GR5.

S. Hayward (2006). Formation and evaporation of regular black holes. PRL 96, 031103.

A. H. Chamseddine & V. Mukhanov (2017). Resolving cosmological singularities. JCAP 03, 009.